

THE DISCOVERY OF BINARY WHITE DWARFS THAT WILL MERGE WITHIN 500 MYR¹

Mukremin Kilic^{2,4}, Warren R. Brown², Carlos Allende Prieto³, and S. J. Kenyon²

ABSTRACT

We present radial velocity observations of four extremely low-mass ($0.2 M_{\odot}$) white dwarfs. All four stars show peak-to-peak radial velocity variations of $540 - 710 \text{ km s}^{-1}$ with $1.0 - 5.9 \text{ hr}$ periods. The optical photometry rules out main-sequence companions. In addition, no milli-second pulsar companions are detected in radio observations. Thus the invisible companions are most likely white dwarfs. Due to the loss of angular momentum through gravitational radiation, three of the systems will merge within 500 Myr. The remaining system will merge within a Hubble time. The mass functions for three of the systems imply companions more massive than $0.44 M_{\odot}$; thus those are carbon/oxygen core white dwarfs. However, the chance of a supernova Ia event is only 1% to 5%. These systems will most likely form single R Coronae Borealis stars, providing evidence for a white dwarf + white dwarf merger mechanism for these unusual objects. One of the systems, SDSS J105353.89+520031.0 has a 70% chance of having a low-mass white dwarf companion. This system will probably form a single helium-enriched subdwarf O star. All four white dwarf systems have unusual mass ratios of $\leq 0.2 - 0.8$ that may also lead to the formation of AM CVn systems. The unknown inclination angles prohibit a definitive conclusion about the future of these systems.

Subject headings: stars: low-mass — white dwarfs — stars: individual (SDSS J082212.57+275307.4, J084910.13+044528.7, J105353.89+520031.0, J143633.29+501026.8)

²Smithsonian Astrophysical Observatory, 60 Garden St., Cambridge, MA 02138, USA

³Mullard Space Science Laboratory, University College London, Holmbury St. Mary, Surrey RH5 6NT, UK

⁴*Spitzer Fellow*; mkilic@cfa.harvard.edu

¹Based on observations obtained at the MMT Observatory, a joint facility of the Smithsonian Institution and the University of Arizona.

1. INTRODUCTION

Mergers of binary white dwarfs (WDs) have been proposed to explain supernovae (SNe) Ia events, extreme helium stars including R Coronae Borealis (RCrB) stars, and single subdwarf B and O stars (Iben & Tutukov 1984; Webbink 1984; Saio & Jeffery 2000, 2002; Heber 2009). However, radial velocity surveys of WDs have not revealed a large binary population that will merge within a Hubble time (Marsh 1995; Maxted et al. 2000; Napiwotzki et al. 2001, 2002; Karl et al. 2003; Nelemans et al. 2005).

Radial velocity observations of extremely low-mass (ELM, $M \sim 0.2 M_{\odot}$) WDs provide a new opportunity to find short period binaries. The Universe is not old enough to produce ELM WDs through single star evolution. These WDs must therefore undergo significant mass loss during their formation in binary systems. The majority of ELM WDs have been identified as companions to milli-second pulsars. However, not all ELM WDs have such companions (van Leeuwen et al. 2007; Agüeros et al. 2009a). Radial velocity, radio, and x-ray observations of the lowest gravity WD found in the Sloan Digital Sky Survey (SDSS), J0917+4638, show that the companion is almost certainly another WD (Kilic et al. 2007a,b; Agüeros et al. 2009b).

Recently, Eisenstein et al. (2006) identified a dozen ELM WDs in the SDSS Data Release 4 area. Here, we present radial velocity observations of four WDs from that sample; SDSS J082212.57+275307.4, SDSS J084910.13+044528.7, SDSS J105353.89+520031.0, and SDSS J143633.29+501026.8. Our observations are discussed in Section 2; an analysis of the spectroscopic data and the nature of the companions are discussed in Section 3. The future of these binary systems and the merger products are discussed in Section 4.

2. OBSERVATIONS

We used the 6.5m MMT equipped with the Blue Channel Spectrograph to obtain moderate resolution spectroscopy of four ELM WDs on UT 2009 March 27-29 and April 1-3. In addition, we observed J0822+2753 on UT 2008 September 23-24. We used a $1''$ slit and the 832 line mm^{-1} grating in second order to obtain spectra with a wavelength coverage of 3600 – 4500 Å and a resolving power of $R = 4300$. We obtained all spectra at the parallactic angle and acquired comparison lamp exposures after every science exposure. We checked the stability of the spectrograph by measuring the centroid of the Hg emission line at 4358.34 Å. We found it to be stable to within 10 km s^{-1} , with an average offset from the rest wavelength of $-0.4 \pm 4.9 \text{ km s}^{-1}$. We flux-calibrated the spectra using blue spectrophotometric standards (Massey et al. 1988).

Brown et al. (2006) observed J1053+5200 in 2006 February as part of their hypervelocity B-star survey. We include this additional MMT spectrum in our analysis to extend the time baseline. We use the cross-correlation package RVSAO (Kurtz & Mink 1998) to measure heliocentric radial velocities. We obtain preliminary velocities by cross-correlating the observations with bright WD templates of known velocity. However, greater velocity precision comes from cross-correlating the objects with themselves. Thus we shift the individual spectra to rest-frame and sum them together into a high signal-to-noise ratio template spectrum for each object. Our final velocities come from cross-correlating the individual observations with these templates, and are presented in Table 1.

We also use WD model spectra with atmospheric parameters customized for each object (see §3) to measure radial velocities. The results are consistent within 10 km s^{-1} . Thus, the systematic errors in our measurements are $\leq 10 \text{ km s}^{-1}$; the mean velocity difference between the analyses is $1.5 \pm 3.7 \text{ km s}^{-1}$. This small uncertainty gives us confidence that the velocities in Table 1 are reliable.

Table 1. Radial Velocity Measurements

Object	HJD +2450000	Heliocentric Radial Velocity (km s ⁻¹)
J0822+2753	4732.98282	-254.7 ± 13.6
...	4732.99047	-303.4 ± 11.9
...	4733.00223	-312.4 ± 13.5
...	4733.97631	-295.7 ± 13.4
...	4733.99015	-238.0 ± 14.1
...	4917.61018	$+216.2 \pm 10.8$
...	4922.62095	-291.8 ± 4.5
...	4922.68488	$+99.5 \pm 4.8$
...	4922.75956	$+97.1 \pm 7.6$
...	4922.79519	-121.5 ± 7.8
...	4923.62620	-148.0 ± 5.3
...	4923.66669	$+128.6 \pm 6.4$
...	4923.70522	$+223.9 \pm 7.3$
...	4923.76270	-60.8 ± 5.9
...	4924.62160	-37.1 ± 8.3
...	4924.74512	-99.8 ± 11.2
J0849+0445	4918.64083	$+415.3 \pm 11.0$
...	4922.64106	$+247.1 \pm 14.1$
...	4922.70390	-195.9 ± 10.4
...	4922.77816	-283.1 ± 11.2
...	4923.64966	-144.7 ± 12.9
...	4923.73361	-12.6 ± 10.9
...	4923.78104	-136.6 ± 12.7
...	4924.64406	-34.2 ± 11.0
...	4924.66382	-292.4 ± 13.5
...	4924.68169	$+189.2 \pm 18.8$
...	4924.70222	$+391.2 \pm 10.3$
...	4924.72610	-142.9 ± 14.9
J1053+5200	3790.79575	-45.2 ± 8.5
...	4919.62596	$+287.6 \pm 8.9$
...	4922.66788	-261.0 ± 9.3
...	4922.74298	$+98.6 \pm 10.4$

3. RESULTS

All four targets display radial velocity variations of $\geq 540 \text{ km s}^{-1}$ between different observations. We weight each velocity by its associated error and solve for the best-fit orbit using the code of Kenyon & Garcia (1986). The heliocentric radial velocities are best fit with circular orbits and with velocity semi-amplitudes $K = 265 - 367 \text{ km s}^{-1}$. The best-fit orbital periods range from 0.0426 to 0.2440 days (1.0 to 5.9 hr). Figures 1-4 show the observed radial velocities and the best fit orbits for our targets. We have velocity data from 3 – 6 nights spread over a time baseline of 3 – 1134 nights. The short orbital periods and relatively long time baseline help us to constrain the orbital periods accurately.

The orbital parameters for our targets including the orbital period, semi-amplitude (K) of the radial velocity variations, systemic velocity, the time of spectroscopic conjunction, and mass function are presented in Table 2. We note that the systemic velocities in this table include a gravitational redshift term, which should be subtracted from these velocities to find the true systemic velocities. This correction is on the order of 3 km s^{-1} for our targets (see the discussion below).

We perform model fits to each individual spectrum and also to the average composite spectra using synthetic DA WD spectra kindly provided by D. Koester. We use the individual spectra to obtain a robust estimate of the errors in our analysis. Figure 5 shows the composite spectra and our fits using the entire wavelength range. The best-fit T_{eff} and $\log g$ values are given in Table 3. We obtain best-fit solutions of $8880 - 16550 \text{ K}$ and $\log g = 6.23 - 6.69$ for our targets, confirming that they are ELM WDs.

Slight differences between the continuum level of the observations and that of the best-fit model spectrum are evident for J1053+5200. These differences are suggestive of an imperfect flux calibration. If we normalize (continuum-correct) the composite spectra and fit just the Balmer lines, we obtain best-fit solutions that differ by $70 - 800 \text{ K}$ in T_{eff} and 0.1 dex in $\log g$ for our four targets. These fits are shown in the right panel of Figure 5. These solutions are consistent with the fits to the entire spectra within the errors. Our T_{eff} estimates are consistent with the Eisenstein et al. (2006) analysis within 500 K , and $\log g$ values within 0.4 dex . Given the higher resolution and higher signal-to-noise ratio MMT data and shorter exposure times, our T_{eff} and $\log g$ estimates (columns 2 and 3 in Table 3) should be more reliable.

Figure 6 shows the effective temperatures and surface gravities for our targets (red circles) plus the previously identified ELM WDs in the literature. Open circles show the WD companions to milli-second pulsars PSR J1012+5307 and J1911-5958A (van Kerkwijk et al. 1996; Bassa et al. 2006). Filled triangles show the ELM sdB star HD 188112 (Heber et al.

Table 1—Continued

Object	HJD +2450000	Heliocentric Radial Velocity (km s ⁻¹)
...	4922.82846	+10.8 ± 7.4
...	4922.91686	−65.2 ± 7.8
...	4923.68895	−220.1 ± 7.8
...	4923.80370	+177.3 ± 7.7
...	4923.87868	+220.5 ± 6.4
...	4924.76454	−45.3 ± 14.0
...	4924.78045	+260.2 ± 13.7
...	4924.79571	−249.6 ± 14.7
...	4924.81573	+235.9 ± 13.5
...	4924.83218	−60.0 ± 13.5
J1436+5010	4922.85253	+301.4 ± 7.4
...	4922.93341	−50.8 ± 11.5
...	4922.98659	+224.2 ± 5.6
...	4923.82133	+230.8 ± 6.8
...	4923.85329	+89.8 ± 6.7
...	4923.89751	+41.9 ± 5.8
...	4923.93904	−188.1 ± 7.0
...	4923.98171	−296.2 ± 6.6
...	4923.99118	+109.6 ± 6.1
...	4924.94756	−140.7 ± 9.3
...	4924.95335	+112.2 ± 11.8
...	4924.96121	+327.2 ± 10.6
...	4924.96700	+243.6 ± 15.9
...	4924.97398	−72.7 ± 11.0
...	4924.97975	−324.1 ± 11.0
...	4924.98684	−372.5 ± 14.0

Table 2. Orbital Parameters

Object	P (days)	K (km s ⁻¹)	Systemic Velocity (km s ⁻¹)	Spectroscopic Conjunction	Mass Function
J0822+2753	0.2440 ± 0.0002	271.1 ± 9.0	−52.2 ± 4.5	2454732.8312	0.5038 ± 0.07745
J0849+0445	0.0787 ± 0.0001	366.9 ± 14.7	47.8 ± 7.4	2454918.6200	0.4026 ± 0.06380
J1053+5200	0.0426 ± 0.0001	264.8 ± 15.0	21.4 ± 7.7	2453790.7977	0.08195 ± 0.01418
J1436+5010	0.0458 ± 0.0001	347.4 ± 8.9	−30.2 ± 5.1	2454922.8430	0.1990 ± 0.02969

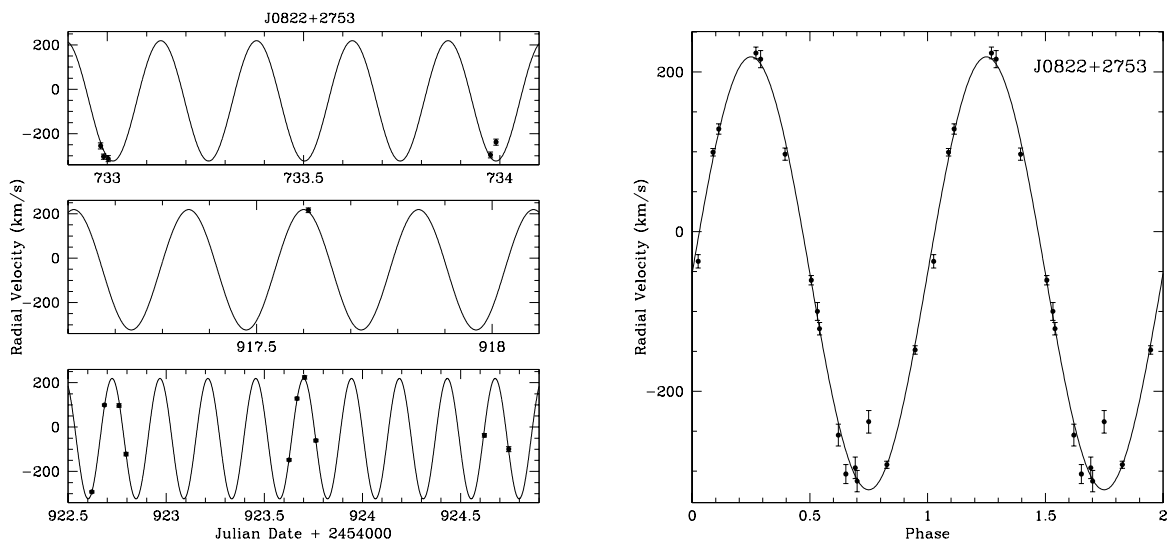


Fig. 1.— The radial velocities of the white dwarf J0822+2753 observed in 2008 September (top left panel), 2009 March (middle left panel) and 2009 April (bottom left panel). The right panel shows all of these data points phased with the best-fit period. The solid line represents the best-fit model for a circular orbit with a radial velocity amplitude of 271.1 km s^{-1} and a period of 0.2440 days.

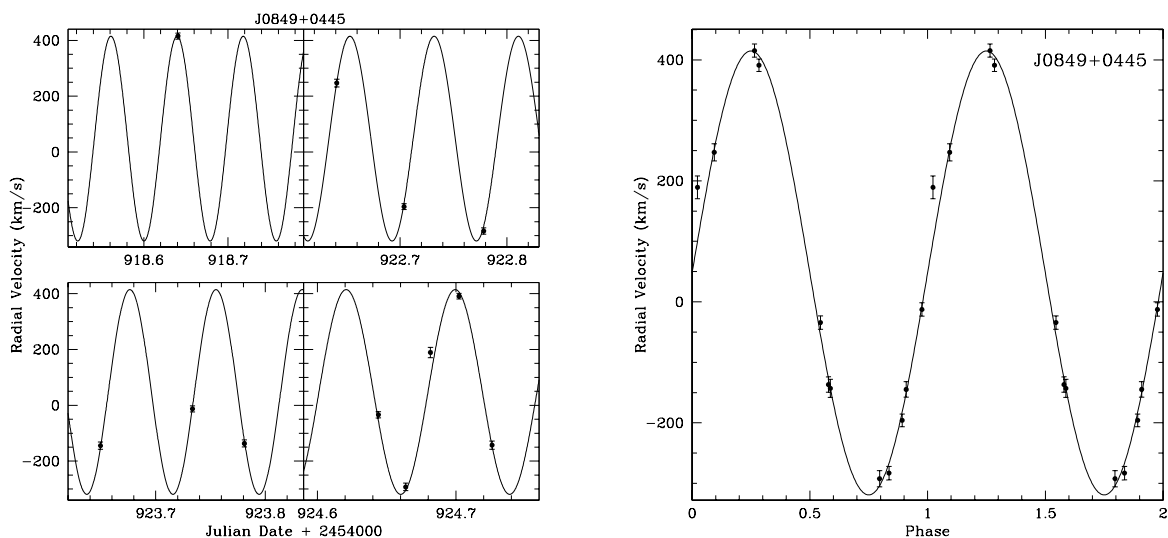


Fig. 2.— The radial velocities of the white dwarf J0849+0445 observed in 2009 March and April (left panels). The right panel shows all of these data points phased with the best-fit period. The solid line represents the best-fit model for a circular orbit with $K = 366.9 \text{ km s}^{-1}$ and $P = 0.0787$ days.

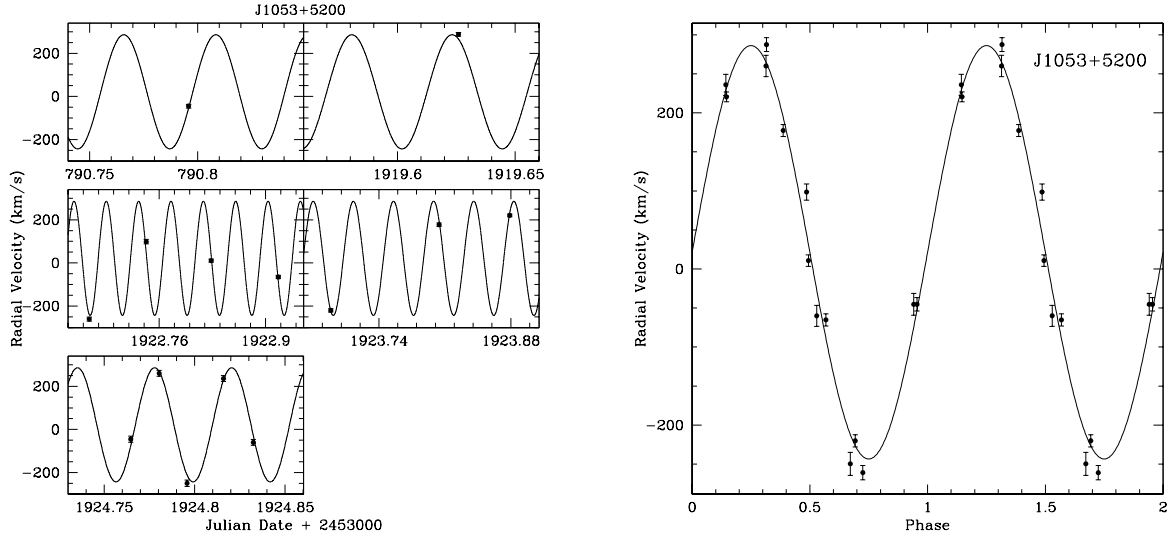


Fig. 3.— The radial velocities of the white dwarf J1053+5200 observed in 2006 February, 2009 March and April (left panels). The right panel shows all of these data points phased with the best-fit period. The solid line represents the best-fit model for a circular orbit with $K = 264.8 \text{ km s}^{-1}$ and $P = 0.0426$ days.

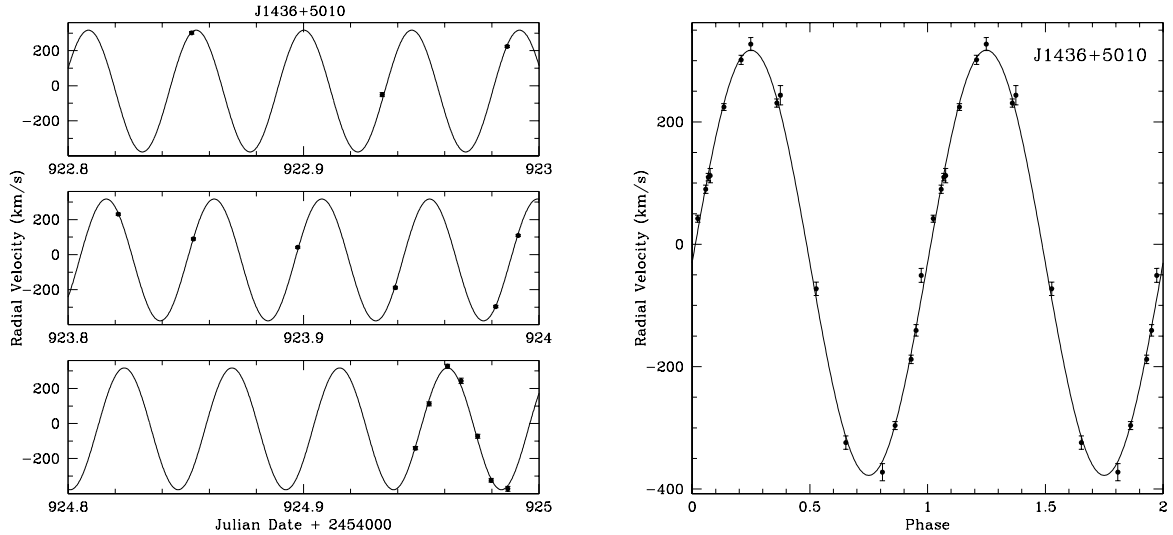


Fig. 4.— The radial velocities of the white dwarf J1436+5010 observed in 2009 April (left panels). The right panel shows all of these data points phased with the best-fit period. The solid line represents the best-fit model for a circular orbit with $K = 347.4 \text{ km s}^{-1}$ and $P = 0.0458$ days.

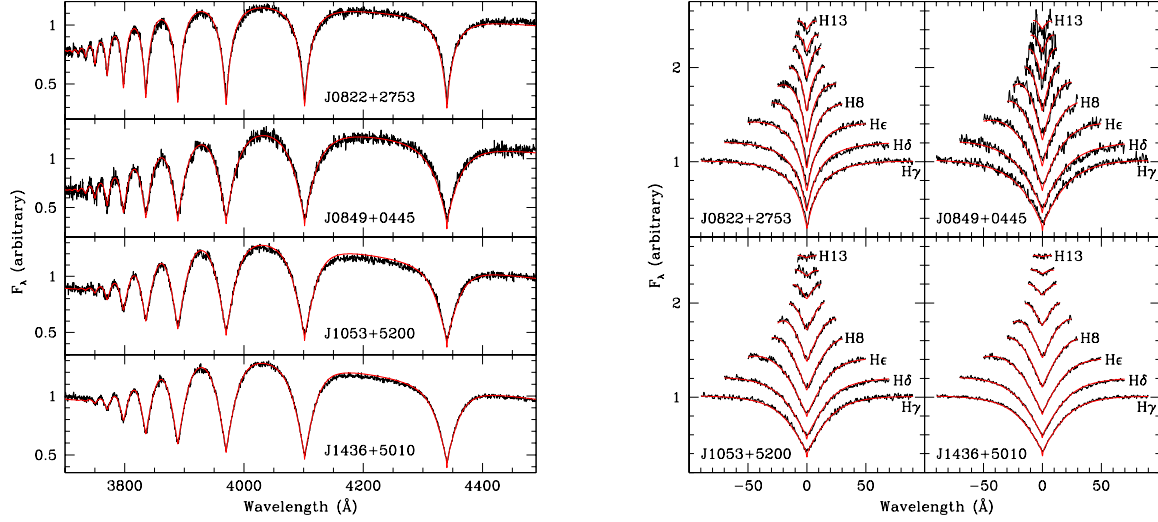


Fig. 5.— Spectral fits (red solid lines) to the composite spectra of our targets (jagged lines, left panels) and to the flux-normalized line profiles (right panels).

Table 3. Physical Parameters

Object	T_{eff} (K)	$\log g$	Mass (M_\odot)	Companion Mass (M_\odot)	$i = 60^\circ$ (M_\odot)	NS Probability	SN Ia Probability	Merger Time (Gyr)
J0822+2753	8880 ± 60	6.44 ± 0.11	0.17	≥ 0.76	1.05	18%	5%	≤ 8.42
J0849+0445	10290 ± 250	6.23 ± 0.08	0.17	≥ 0.64	0.88	15%	4%	≤ 0.47
J1053+5200	15180 ± 600	6.55 ± 0.09	0.20	≥ 0.26	0.33	4%	1%	≤ 0.16
J1436+5010	16550 ± 260	6.69 ± 0.07	0.22	≥ 0.44	0.58	9%	4%	≤ 0.12

2003), and the WDs SDSS J0917+4638 (Kilic et al. 2007a,b) and LP400–22 (Kawka et al. 2006; Kilic et al. 2009; Vennes et al. 2009). All of these WDs show radial velocity variations. Solid lines show the constant mass tracks for low mass WDs from Althaus et al. (2001, labeled in M_{\odot} on the right side of the figure) and the tracks for zero age main-sequence and horizontal branch stars. The difference between the low mass WD models below and above $0.18 M_{\odot}$ is caused by element diffusion and thermonuclear flashes. The models with $M < 0.18 M_{\odot}$ do not experience thermonuclear flashes. As a result, they have massive hydrogen envelopes, larger radii, and lower surface gravities.

Figure 6 shows that both J0822+2753 and J0849+0445 are $\approx 0.17 M_{\odot}$ WDs, whereas J1053+5200 and J1436+5010 are $0.20 M_{\odot}$ and $0.22 M_{\odot}$ WDs, respectively.

4. DISCUSSION

4.1. J0822+2753

The temperature and surface gravity for J0822+2753 imply an absolute magnitude of $M_V \approx 9.6$, a radius of $0.04 R_{\odot}$, and an age of 2.8 Gyr (Althaus et al. 2001). This luminosity places it at a distance of 600 pc, 330 pc above the plane. J0822+2753 has a proper motion of $\mu_{\alpha} \cos \delta = 3.4 \pm 3.5$ and $\mu_{\delta} = -19.2 \pm 3.5$ mas yr $^{-1}$ (Munn et al. 2004). Based on the mass and radius estimates, the gravitational redshift of the WD is 2.6 km s^{-1} . Therefore, the true systemic velocity is -54.6 km s^{-1} . The velocity components with respect to the local standard of rest as defined by Hogg et al. (2005) are $U = 67 \pm 7$, $V = -38 \pm 11$, and $W = -27 \pm 9 \text{ km s}^{-1}$. Clearly, J0822+2753 is a disk star (Chiba & Beers 2000).

We combine the spectra near maximum blue-shifted radial velocity and near minimum radial velocity into two composite spectra. If there is a contribution from a companion object, it may be visible as an asymmetry in the line profiles. We do not see any obvious asymmetries in the line profiles and conclude that our optical spectroscopy does not reveal any spectral features from a companion object. A main-sequence star companion with $M \geq 0.76 M_{\odot}$ would have $M_I < 6.5 \text{ mag}$ (Kroupa & Tout 1997), brighter than the low-mass WD ($M_I \approx 9.3 \text{ mag}$) and detectable in the I -band.

Figure 7 shows the SDSS photometry of our targets compared to WD model predictions. It is clear from this figure that none of the targets in our sample, including J0822+2753, shows excess flux in the optical. Hence, a main-sequence star companion is ruled out for J0822+2753.

Using the mean inclination angle for a random stellar sample, $i = 60^{\circ}$, we estimate that

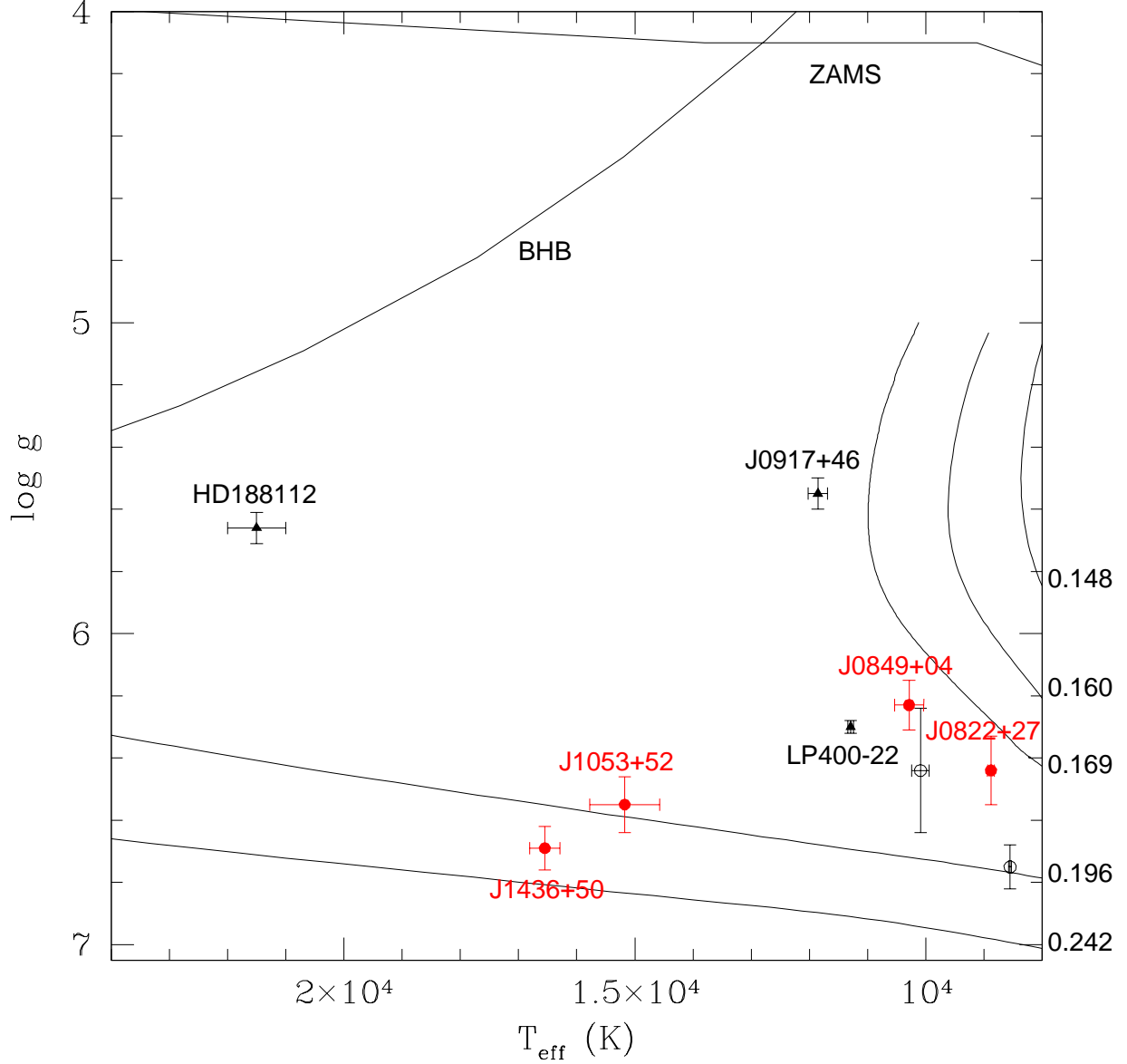


Fig. 6.— The best fit solutions for the surface gravity and temperatures of our targets (filled circles), overlaid on tracks of constant mass from Althaus et al. (2001). Zero-age main-sequence (ZAMS) and horizontal branch star (BHB) tracks are also shown. Spectroscopically confirmed ELM WDs and sdBs found in the literature are shown as filled triangles. Companions to milli-second pulsars PSR J1012+5307 and J1911-5958A are shown as open circles.

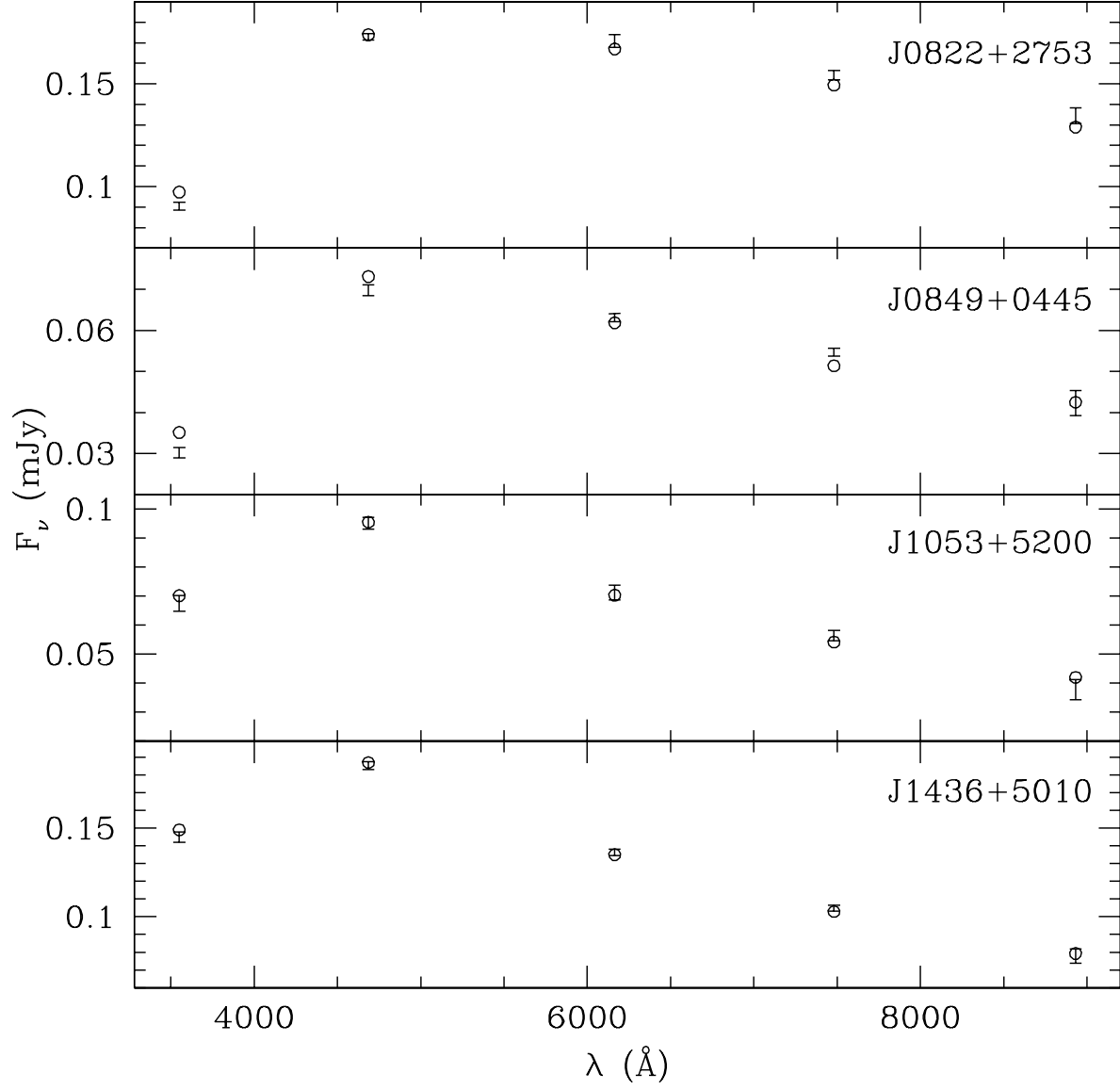


Fig. 7.— Spectral energy distributions of our targets (error bars) and the WD model predictions (open circles).

the companion is likely a $1.05 M_{\odot}$ object at an orbital separation of $1.8 R_{\odot}$. This separation is about $40\times$ larger than the radius of the WD. The probability of a neutron star companion, i.e. $M = 1.4 - 3.0 M_{\odot}$, is 18%. Agüeros et al. (2009a) obtained radio observations of all four of our targets, including J0822+2753, using the Green Bank Telescope. They do not see any evidence of a milli-second pulsar companion. Therefore, the companion is most likely a massive WD. However, follow-up x-ray observations are required to rule out a neutron star companion.

4.2. J0849+0445

Based on its temperature and surface gravity, we estimate that J0849+0445 is 1.3 Gyr old, and it has $M_V = 8.4$ mag and $R = 0.05 R_{\odot}$. Its distance is 1.6 kpc, 780 pc above the plane. Its proper motion is consistent with zero (Munn et al. 2004). The gravitational redshift of the WD is 2.1 km s^{-1} . Hence, the true systemic velocity is 45.7 km s^{-1} . The velocity components with respect to the local standard of rest are $U = -22 \pm 21$, $V = -25 \pm 22$, and $W = 23 \pm 24 \text{ km s}^{-1}$. J0849+0445 is also a disk star.

As in the case of J0822+2753, we do not see any evidence of a companion in our spectra. Main-sequence companions are ruled out based on the SDSS photometry. In addition, radio observations do not reveal a milli-second pulsar companion. There is a 70% probability that the companion is less massive than $1.4 M_{\odot}$. Therefore, the companion is most likely another WD with $M \geq 0.64 M_{\odot}$. Assuming an inclination angle of 60° , we estimate that the companion is probably a $0.88 M_{\odot}$ object at $0.8 R_{\odot}$ (or $15 \times R_{WD}$) separation.

4.3. J1053+5200

J1053+5200 has $M = 0.20 M_{\odot}$, $R = 0.04 R_{\odot}$, and $M_V = 8.9$ mag. This absolute magnitude corresponds to a WD cooling age of 430 Myr (Althaus et al. 2001). Its distance is 1.2 kpc, 1 kpc above the plane. It has a proper motion of $\mu_{\alpha} \cos \delta = -29.7 \pm 3.5$ and $\mu_{\delta} = -31.2 \pm 3.5 \text{ mas yr}^{-1}$ (Munn et al. 2004). The gravitational redshift of the WD is 3.2 km s^{-1} . The velocity components with respect to the local standard of rest are $U = -118 \pm 20$, $V = -206 \pm 30$, and $W = 7 \pm 13 \text{ km s}^{-1}$. J1053+5200 lags behind the Galactic disk and is clearly a halo star.

The mass function for J1053+5200 implies that the companion is more massive than $0.26 M_{\odot}$. A $0.26 M_{\odot}$ main-sequence star would be about 50% fainter than the WD in the I -band and it would have been detected in the SDSS i - and z - band data. The lack of

excess flux in the SDSS photometry (Figure 7) rules out a main-sequence companion. A neutron star companion is unlikely (4% probability). The companion is most likely another WD, and specifically a low-mass ($M < 0.45 M_{\odot}$) WD. J1053+5200 has a 70% chance of having a low-mass WD companion. Assuming an inclination angle of 60° , we estimate that the companion is probably a low mass object with $M = 0.33 M_{\odot}$ at $0.4 R_{\odot}$ separation.

4.4. J1436+5010

J1436+5010 has $M \approx 0.22 M_{\odot}$. Interpolating the Althaus et al. (2001) models for 0.2 and $0.24 M_{\odot}$ models, we estimate that J1436+5010 is a 100 – 400 Myr old WD at a distance of ≈ 870 pc, 770 pc above the Galactic plane. The gravitational redshift of the WD is 4.0 km s^{-1} . It has a proper motion of $\mu_{\alpha} \cos \delta = 7.8 \pm 3.5$ and $\mu_{\delta} = -5.1 \pm 3.5 \text{ mas yr}^{-1}$ (Munn et al. 2004). The velocity components with respect to the local standard of rest are $U = 47 \pm 15$, $V = -4 \pm 13$, and $W = -29 \pm 9 \text{ km s}^{-1}$. J1436+5010 is a disk object.

We do not see any evidence of a companion in our MMT spectra of this object. In addition, the companion has to be more massive than $0.44 M_{\odot}$, and such a main-sequence star companion is ruled out based on the SDSS photometry data. There is a 9% chance that the companion is a neutron star. However, the companion is most likely a carbon/oxygen core WD. Assuming an inclination angle of 60° , we estimate that the companion is probably a $0.58 M_{\odot}$ object at $0.5 R_{\odot}$ ($14 \times R_{WD}$) separation.

Ramírez et al. (2007) used Gaussian probability distributions to assign stars to the different Galactic components based on kinematics. Using the same criterion, J1436+5010 and J0849+0445 have 97% and 3% chances of being thin and thick disk members, respectively. J0822+2753 has an 81% chance of being a thin disk member and 19% chance of a thick disk membership. On the other hand, J1053+5200 has a 99.7% chance of being a halo member. These statistics confirm our membership assignments presented above.

5. THE COMMON-ENVELOPE PHASE

Our radial velocity observations and the available optical photometry show that none of our targets have main-sequence companions. The probability of neutron star companions ($M > 1.4 M_{\odot}$) ranges from 4% to 18%. However, no such companions are visible in the radio data (Agüeros et al. 2009a). Therefore, the companions are most likely other WDs.

The formation scenarios for close WD pairs include two consecutive common-envelope phases or an Algol-like stable mass transfer phase followed by a common-envelope phase

(Iben et al. 1997). The mass ratios ($q = M_{\text{bright}}/M_{\text{dim}}$) for our targets range from 0.22 to 0.77, and they favor a scenario involving two common-envelope phases (see Nelemans et al. 2000, and references therein).

Nelemans & Tout (2005) find that the standard common-envelope formalism (the α -formalism) demanding energy balance in the system does not work. Instead, they suggest that the common-envelope evolution of close WD binaries can be reconstructed with an algorithm (γ -algorithm) imposing angular momentum balance. Studying the prior evolution of 10 WD+WD binaries where both WD masses are known, Nelemans et al. (2005) find that the γ -algorithm is able to explain the observed properties of those systems following two common-envelope phases. Most of the systems can be explained with a single-valued $\gamma = 1.5$, where γ is the rate of angular momentum loss as defined by Paczyński & Ziółkowski (1967). The mass ratios of these 10 systems are on the order of unity.

Kilic et al. (2007b) and Kilic et al. (2009) used the γ -algorithm to study the prior evolution of the ELM WD systems J0917+4638 and LP400–22. These two systems have mass ratios of ≤ 0.61 and ≤ 0.46 , respectively. Kilic et al. (2007b) find that the J0917+4638 system can be explained as the descendant of a binary system including a 2.2 and a 0.8 M_{\odot} star at an orbital separation of 0.4 AU. A similar study of the LP400–22 system shows that $\gamma = 1.5$ cannot explain the first common-envelope phase evolution of this binary (Kilic et al. 2009).

Using the same algorithm with $\gamma = 1.5$, we are able to reconstruct the most recent common-envelope phase evolution of our targets. Assuming an inclination angle of 60° , we estimate that a common-envelope phase involving a 2.2 and a 1.05 M_{\odot} star at an orbital separation of 5.9 R_{\odot} can explain the binary J0822+2753 as observed today. Similarly, a 2.0 + 0.88 M_{\odot} binary at 5.8 R_{\odot} separation, a 1.1 + 0.33 M_{\odot} binary at 10.5 R_{\odot} separation, and a 1.6 + 0.58 M_{\odot} binary at 15.7 R_{\odot} separation can explain the J0849+0445, J1053+5200, and J1436+5010 binary systems, respectively. The companions would be older and fainter than the 0.17 – 0.22 M_{\odot} WDs observed today, consistent with the lack of evidence for the presence of companions in the SDSS photometry and our optical spectroscopy.

Using the same algorithm to re-create the first common-envelope phase evolution of our targets, we do not find any solutions involving stars less massive than 2.3 M_{\odot} . This limit is set by the fact that more massive stars do not form degenerate helium cores and that a common-envelope phase with a more massive giant would end up in a merger and not in a binary system (Nelemans et al. 2000). With mass ratios ranging from 0.22 to 0.77, our four targets plus J0917+4638 and LP400–22 binary systems provide new constraints on the role of energy versus angular momentum balance in reconstructing common-envelope phase evolution. However, a full evaluation of the α - and γ -algorithms is beyond the scope of this

paper.

6. THE FUTURE: MERGER PRODUCTS

Short period binaries may merge within a Hubble time by losing angular momentum through gravitational radiation. The merger time for such binaries is

$$\tau = \frac{(M_1 + M_2)^{1/3}}{M_1 M_2} P^{8/3} \times 10^7 \text{yr} \quad (1)$$

where the masses are in solar units and the period is in hours (Landau & Lifshitz 1958; Marsh 1995). For minimum mass companions ($i = 90^\circ$) the merger times for our targets (in right ascension order) are 8420 , 470, 160, and 120 Myr, respectively. All four targets will merge within a Hubble time. We now explore possible outcomes of the merger process.

6.1. EXTREME HELIUM STARS

Hydrogen-deficient luminous stars, in order of decreasing effective temperature, include extreme helium, RCrB, and hydrogen-deficient carbon stars. Studies of the chemical compositions of these stars suggest that they form an evolutionary sequence (García-Hernández et al. 2009). There are two leading scenarios to explain the origin of extreme helium stars. In one scenario, the merger of a He-core WD with a carbon/oxygen core WD forms a hydrogen-deficient supergiant (Webbink 1984; Iben & Tutukov 1984; Saio & Jeffery 2002). The other scenario, commonly referred to as the born-again scenario, suggests that a hydrogen-deficient star forms when a post-asymptotic giant branch star experiences a late helium shell flash (Iben et al. 1996). This flash converts the hydrogen-rich envelope to helium, creating a hydrogen-deficient star.

Studies of elemental and isotopic abundances for carbon, nitrogen, and oxygen are useful for differentiating between these two scenarios. Based on the observed abundances, Saio & Jeffery (2002) and Pandey et al. (2006) argue that most hydrogen-deficient carbon stars and RCrB stars form through WD mergers. In addition, Clayton et al. (2007) find that every RCrB and hydrogen-deficient carbon star that they have observed has enhanced $^{18}\text{O}/^{16}\text{O}$ ratios compared to the solar value. They propose the WD merger scenario as a likely formation mechanism. Based on preliminary calculations, Clayton et al. (2007) find that the accretion of the helium WD by the carbon/oxygen WD is rapid and it induces nucleosynthesis, which converts ^{14}N to ^{18}O by α -capture.

The overproduction of ^{18}O is not predicted in the born-again scenario, because either the ^{14}N is burnt to ^{22}Ne or ^{18}O is destroyed by proton capture (García-Hernández et al. 2009). There is at least one star² identified as a product of the born-again scenario (see Clayton et al. 2006; Miller Bertolami & Althaus 2007, and references therein), Sakurai’s object (V4334 Sgr). Therefore, not all extreme helium stars form through WD mergers.

Three of the ELM WDs in our sample, J0822+2753, J0849+0445, and J1436+5010, have companions more massive than $0.44 M_{\odot}$. These 3 systems most likely have carbon/oxygen WD companions. They will merge within 120 Myr to 8.4 Gyr and form extreme helium stars. Therefore, these 3 systems provide independent evidence that there is a mechanism to form hydrogen deficient stars through WD mergers.

6.2. SINGLE HOT SUBDWARF STARS

Close binary evolution plays an important role in the formation of subdwarf B stars, as witnessed by the large fraction ($\geq 40\%$) of sdB stars in binaries. Mass transfer between the companions and common-envelope evolution can lead to large amount of mass loss prior to the start of core He-burning, creating an sdB star in a binary. Castellani & Castellani (1993) demonstrated that if low-mass stars lose enough mass on the red giant branch, they can depart the red giant branch before the core He flash. Instead, the He flash happens on the hot WD cooling track. Depending on when this flash happens, sdB or He-enriched sdO stars form.

Only about 4% of He-enriched sdO stars are in binary systems (Napiwotzki et al. 2004). Han et al. (2003) argue that the mergers of two He-core WDs can explain the lower fraction of binaries observed among the He-enriched sdO stars. With shrinking separation, the less massive object is accreted onto the companion, leading to He ignition (Heber 2009). Saio & Jeffery (2000) argue that the merger product will be enriched in CNO, similar to the observed abundances of He-enriched sdO stars.

In addition to the merger scenario, single hot subdwarf stars can also be produced through a common-envelope phase with a massive planet or a brown dwarf. The recent discoveries of planets around the subdwarf B stars V Pegasi (Silvotti et al. 2007) and HD 149382 (Geier et al. 2009) show that this channel of formation contributes to the single subdwarf B star population.

There is a 70% chance that the companion to one of our targets, J1053+5200, is a

²Two more have been discussed extensively in the literature, FG Sge and V605 Aql.

low-mass He-core WD. The merger of this binary WD system will most likely create a He-enriched sdO star. Hence, binary mergers of two He-core WDs contribute to the single hot subdwarf population in the Galaxy.

6.3. SNe Ia

SNe Ia are caused by the thermonuclear explosion of WDs growing to the Chandrasekhar mass either by accretion from a companion or by mergers of two degenerate stars. The double degenerate scenario requires mainly mergers of two CO WDs to have sufficient mass to exceed the Chandrasekhar mass limit (Webbink 1984; Iben & Tutukov 1984). However, if the mass transfer is stable and the combined mass is larger than the Chandrasekhar limit, the mergers of CO WDs with low-mass He-core WDs can also create SNe Ia explosions. The population synthesis models by Yungelson (2005) demonstrate that the expected contribution of He+CO WD mergers to the SNe Ia rate is two orders of magnitude smaller than that of the CO+CO WD mergers.

The visible components of the four binaries discussed in this paper are 0.17-0.22 M_{\odot} WDs. There is a 1-5% chance that the companions are massive WDs and the total mass of the binary systems exceed 1.4 M_{\odot} (see Table 3). Our targets are most likely not SNe Ia progenitors.

6.4. WHITE DWARF + NEUTRON STAR MERGERS

Green Bank Telescope observations do not detect milli-second pulsar companions around our targets. However, neutron star companions cannot be ruled out based on the radio data alone. X-ray observations can detect the blackbody emission from a neutron star companion even if it is radio-quiet or if its pulsar beam misses our line of sight. XMM-Newton observations of the extremely low mass WD, SDSS J0917+4638, do not detect a neutron star in the system (Agüeros et al. 2009b). Similar observations will be necessary to search for neutron star companions in our targets.

Based on the mass function, there is a 4-18% chance that the companions to our targets are neutron stars. García-Berro et al. (2007) study the evolution of a 1.4 M_{\odot} neutron star and a 0.6 M_{\odot} merger using a smooth particle hydrodynamics code. They find that, once the white dwarf has filled its Roche lobe, it is disrupted in a few orbital periods, e.g. on the order of 5 minutes. The final configuration consists of a neutron star surrounded by an accretion disk, and the mass loss from the system is negligible. If the companions to our

targets are neutron stars, the merger process would create slightly heavier neutron stars. Given the relatively short distances to our targets, such mergers will be easily detected with gravitational wave detectors like LISA.

6.5. AN ALTERNATIVE FUTURE: AM CVn SYSTEMS

AM CVn stars are interacting double stars with WD or neutron star accretors with orbital periods less than about one hour. Nelemans et al. (2009) propose three formation scenarios for AM CVn systems involving three types of donor stars; WDs, helium stars, or evolved main-sequence stars. Studying the CNO and He abundances of known AM CVn systems, they find evidence of WD donors in some systems, and evolved helium star donors in others.

The WD channel requires a binary system with short enough orbital period that gravitational wave radiation drives the stars into contact. The low-mass WD fills its Roche lobe and transfers mass to the companion. Depending on the mass ratio of the binary system (if the mass ratio is small), the mass transfer is stable and the system evolves to longer periods (see Marsh et al. 2004; Nelemans et al. 2009, and references therein). Marsh et al. (2004) argue that despite the absence of a single system of extreme mass ratio amongst the observed close double WD population, this channel of formation is probable.

Here, we have uncovered four binary systems with extreme mass ratios of ≤ 0.22 to ≤ 0.77 . The important question is whether these systems will merge or if they will instead create AM CVn systems. Marsh et al. (2004) suggest that the mass transfer between double WDs can be dynamically stable, unstable, or the intermediate case of either stability or instability depending on the degree of spin-orbit coupling. The unknown inclination angle for our targets mean that all of our targets fall into this intermediate regime. Therefore, depending on the mass ratio of the systems, these WDs may end up as AM CVn systems.

7. CONCLUSIONS

Almost all known double WD systems have mass ratios on the order of unity. There is only one system in the Nelemans et al. (2005) sample of known binary WDs with a mass ratio of less than 1. Recently, Kilic et al. (2007b, 2009) identified two WD binary systems with mass ratios ≤ 0.6 . However, these two systems (SDSS J0917 and LP400–22) will not merge within a Hubble time.

The four binary systems discussed in this paper will merge within a Hubble time. They

have extreme mass ratios and are likely progenitors of RCrB stars, single He-enriched sdO stars, or AM CVn stars. These systems may even contribute to the SNe Ia population, but the probability of this possibility is small.

Liebert et al. (2005) estimate that the low-mass ($M < 0.45M_{\odot}$) WDs make up about 10% of the local WD population, corresponding to a formation rate of $4 \times 10^{-14} \text{ pc}^{-3} \text{ yr}^{-1}$. Eisenstein et al. (2006) discovered only 13 ELM WDs out of a sample of 9316 WDs found in a survey volume of $\geq 4 \text{ kpc}^3$ in the SDSS Data Release 4 footprint. ELM WDs are rare, they make up about 0.14% of the local WD sample. Of course, the SDSS spectroscopic sample suffers from incompleteness issues, but taken at face value, 0.14% corresponds to a formation rate of $6 \times 10^{-16} \text{ pc}^{-3} \text{ yr}^{-1}$. However, all four ELM WDs discussed in this paper are going to merge within a Hubble time, and some within the next few hundred Myr. Therefore, the formation rate of ELM WDs may be higher by an order of magnitude. For the SDSS DR4 survey volume of 4 kpc^3 , we estimate a formation rate of $0.2 - 2 \times 10^{-5} \text{ yr}^{-1}$. Bogomazov & Tutukov (2009) estimate a CO+He WD merger rate of $6-8 \times 10^{-3} \text{ yr}^{-1}$. The ELM WD mergers discussed in this paper contribute only a small fraction to the overall CO+He WD merger rate in the Galaxy. Yungelson (2005) estimate a SNe Ia occurrence rate of 10^{-5} yr^{-1} from CO+He WD progenitors. Our estimate of the formation rate of ELM WDs is similar to this result.

We present the radial velocity data for four stars in this paper. However, we are obtaining radial velocity observations for the remaining ELM WDs in the Eisenstein et al. (2006) sample. To date, almost all of these ELM WDs show significant radial velocity variations indicating the presence of a companion star. We are continuing to follow-up these objects at the MMT to constrain their orbital periods accurately. The importance of these observations is that, we not only find short period binaries that will merge within a Hubble time, but also the majority of the binaries have extreme mass ratios. Understanding the prior history of these systems require an understanding of the common envelope phase. Studying the mass ratios and physical characteristics of these systems will be useful for constraining the energy or momentum balance algorithms that are used to reconstruct the evolution of close binary pairs.

Support for this work was provided by NASA through the *Spitzer Space Telescope* Fellowship Program, under an award from Caltech. MK thanks M. Agüeros for helpful discussions and D. Steeghs for discussions on the formation channels for AM CVn stars.

Facilities: MMT (Blue Channel Spectrograph)

REFERENCES

- Agüeros, M. A., Camilo, F., Silvestri, N. M., Kleinman, S. J., Anderson, S. F., & Liebert, J. W. 2009a, *ApJ*, 697, 283
- Agüeros, M. A., et al. 2009b, *ApJ*, 700, L123
- Althaus, L. G., Serenelli, A. M., & Benvenuto, O. G. 2001, *MNRAS*, 323, 471
- Bassa, C. G., van Kerkwijk, M. H., Koester, D., & Verbunt, F. 2006, *A&A*, 456, 295
- Bogomazov, A. I., & Tutukov, A. V. 2009, *Astronomy Reports*, 53, 214
- Brown, W. R., Geller, M. J., Kenyon, S. J., & Kurtz, M. J. 2006, *ApJ*, 647, 303
- Castellani, M., & Castellani, V. 1993, *ApJ*, 407, 649
- Chiba, M., & Beers, T. C. 2000, *AJ*, 119, 2843
- Clayton, G. C., Kerber, F., Pirzkal, N., De Marco, O., Crowther, P. A., & Fedrow, J. M. 2006, *ApJ*, 646, L69
- Clayton, G. C., Geballe, T. R., Herwig, F., Fryer, C., & Asplund, M. 2007, *ApJ*, 662, 1220
- Eisenstein, D. J., et al. 2006, *ApJS*, 167, 40
- García-Berro, E., Pedemonte, A. G., García-Senz, D., Lorén-Aguilar, P., Isern, J., & Lobo, J. A. 2007, *Journal of Physics Conference Series*, 66, 012040
- García-Hernández, D. A., Hinkle, K. H., Lambert, D. L., & Eriksson, K. 2009, *ApJ*, 696, 1733
- Geier, S., Edelmann, H., Heber, U., & Morales-Rueda, L. 2009, *ApJ*, 702, L96
- Han, Z., Podsiadlowski, P., Maxted, P. F. L., & Marsh, T. R. 2003, *MNRAS*, 341, 669
- Heber, U., Edelmann, H., Lisker, T., & Napiwotzki, R. 2003, *A&A*, 411, L477
- Heber, U. 2009, *Annual Review of Astronomy and Astrophysics*, 47
- Hogg, D. W., Blanton, M. R., Roweis, S. T., & Johnston, K. V. 2005, *ApJ*, 629, 268
- Iben, I., Jr., & Tutukov, A. V. 1984, *ApJS*, 54, 335
- Iben, I. J., Tutukov, A. V., & Yungelson, L. R. 1996, *ApJ*, 456, 750

- Iben, I. J., Tutukov, A. V., & Yungelson, L. R. 1997, *ApJ*, 475, 291
- Karl, C. A., Napiwotzki, R., Nelemans, G., Christlieb, N., Koester, D., Heber, U., & Reimers, D. 2003, *A&A*, 410, 663
- Kenyon, S. J. & Garcia, M. R. 1986, *AJ*, 91, 125
- Kawka, A., Vennes, S., Oswalt, T. D., Smith, J. A., & Silvestri, N. M. 2006, *ApJ*, 643, L123
- Kilic, M., Allende Prieto, C., Brown, W. R., & Koester, D. 2007a, *ApJ*, 660, 1451
- Kilic, M., Brown, W. R., Allende Prieto, C., Pinsonneault, M. H., & Kenyon, S. J. 2007b, *ApJ*, 664, 1088
- Kilic, M., Brown, W. R., Allende Prieto, C., Swift, B., Kenyon, S. J., Liebert, J., & Agüeros, M. A. 2009, *ApJ*, 695, L92
- Kroupa, P., & Tout, C. A. 1997, *MNRAS*, 287, 402
- Kurtz, M. J., & Mink, D. J. 1998, *PASP*, 110, 934
- Landau, L. & Lifshitz, E. 1958, *The Theory of Classical Fields*, Pergamon Press, Oxford
- Liebert, J., Bergeron, P., & Holberg, J. B. 2005, *ApJS*, 156, 47
- Marsh, T. R. 1995, *MNRAS*, 275, L1
- Marsh, T. R., Nelemans, G., & Steeghs, D. 2004, *MNRAS*, 350, 113
- Massey, P., Strobel, K., Barnes, J. V., & Anderson, E. 1988, *ApJ*, 328, 315
- Maxted, P. F. L., Marsh, T. R., & Moran, C. K. J. 2000, *MNRAS*, 319, 305
- Miller Bertolami, M. M., & Althaus, L. G. 2007, *MNRAS*, 380, 763
- Munn, J. A., et al. 2004, *AJ*, 127, 3034
- Napiwotzki, R., Edelmann, H., Heber, U., Karl, C., Drechsel, H., Pauli, E.-M., & Christlieb, N. 2001, *A&A*, 378, L17
- Napiwotzki, R., et al. 2002, *A&A*, 386, 957
- Napiwotzki, R., Karl, C. A., Lisker, T., Heber, U., Christlieb, N., Reimers, D., Nelemans, G., & Heuer, D. 2004, *Ap&SS*, 291, 321
- Nelemans, G., Verbunt, F., Yungelson, L. R., & Portegies Zwart, S. F. 2000, *A&A*, 360, 1011

- Nelemans, G., et al. 2005, *A&A*, 440, 1087
- Nelemans, G., & Tout, C. A. 2005, *MNRAS*, 356, 753
- Nelemans, G., Yungelson, L. R., van der Sluys, M. V., & Tout, C. A. 2009, *MNRAS*, in pres, arXiv:0909.3376
- Paczyński, B., & Ziółkowski, J. 1967, *Acta Astronomica*, 17, 7
- Pandey, G., Lambert, D. L., Jeffery, C. S., & Rao, N. K. 2006, *ApJ*, 638, 454
- Ramírez, I., Allende Prieto, C., & Lambert, D. L. 2007, *A&A*, 465, 271
- Ritter, H., & Kolb, U. 2003, *A&A*, 404, 301
- Saio, H., & Jeffery, C. S. 2000, *MNRAS*, 313, 671
- Saio, H., & Jeffery, C. S. 2002, *MNRAS*, 333, 121
- Silvotti, R., et al. 2007, *Nature*, 449, 189
- van Kerkwijk, M. H., Bergeron, P., & Kulkarni, S. R. 1996, *ApJ*, 467, L89
- van Leeuwen, J., Ferdman, R. D., Meyer, S., & Stairs, I. 2007, *MNRAS*, 374, 1437
- Vennes, S., Kawka, A., Vaccaro, T. R., & Silvestri, N. M. 2009, *A&A*, in press, arXiv:0909.3261
- Webbink, R. F. 1984, *ApJ*, 277, 355
- Yungelson, L. R. 2005, *White dwarfs: cosmological and galactic probes*, 332, 163